

See discussions, stats, and author profiles for this publication at: <https://www.researchgate.net/publication/306099733>

Enhancing the Bandwidth of DACs by Analog Bandwidth Interleaving

Conference Paper · April 2016

CITATIONS

18

READS

4,485

4 authors:



Christian Schmidt

Fraunhofer-Institut für Nachrichtentechnik, Heinrich-Hertz-Institut

24 PUBLICATIONS 262 CITATIONS

[SEE PROFILE](#)



Christoph Kottke

Fraunhofer-Gesellschaft zur Förderung der angewandten Forschung e.V.

78 PUBLICATIONS 2,207 CITATIONS

[SEE PROFILE](#)



Volker Jungnickel

Fraunhofer-Institut für Nachrichtentechnik, Heinrich-Hertz-Institut

338 PUBLICATIONS 7,826 CITATIONS

[SEE PROFILE](#)



Ronald Freund

Fraunhofer-Institut für Nachrichtentechnik, Heinrich-Hertz-Institut

116 PUBLICATIONS 1,871 CITATIONS

[SEE PROFILE](#)

Enhancing the Bandwidth of DACs by Analog Bandwidth Interleaving

Christian Schmidt^{1,2}, Christoph Kottke^{1,2}, Volker Jungnickel¹, Ronald Freund¹

¹ Fraunhofer Heinrich Hertz Institut, Einsteinufer 37, 10587 Berlin, Germany

² Technische Universität Berlin, Straße des 17. Juni 135, 10623 Berlin, Germany

christian.schmidt@hhi-extern.fraunhofer.de

Abstract

The rising demand for high-speed data transmission systems requires the upgrade of existing fiber-optic transport networks. A key component of nowadays fiber optics links are fast digital-to-analog converters (DACs), which are mainly limited by their bandwidth. We present a novel concept called *analog bandwidth interleaving* to increase the bandwidth of DACs by interleaving multiple DACs in the frequency domain. A multiple-input multiple-output (MIMO) digital signal processing (DSP) algorithm is presented undoing the crosstalk between the frequency bands. Moreover, the concept is validated experimentally using two low-speed DACs.

Kurzfassung

Die steigende Nachfrage nach Hochgeschwindigkeitsdatenübertragungssystemen erfordert die Erweiterung der existierenden faser-optischen Netzwerke. Eine Schlüsselkomponente heutiger faser-optischer Links sind schnelle Digital-zu-Analog-Wandler (DACs), die hauptsächlich durch ihre Bandbreite limitiert sind. Wir präsentieren ein neues Konzept namens *Analog Bandwidth Interleaving*, um die Bandbreite von DACs durch das verschachtelte Zusammensetzen von mehreren DACs im Frequenzbereich zu erhöhen. Es wird ein Mehrgrößen- (MIMO) Algorithmus vorgestellt, der das Übersprechen zwischen den Frequenzbändern kompensiert. Schließlich wird das Konzept experimentell mit zwei DACs validiert.

1 Introduction

The increasing need for high data rates raises the requirements for high-speed communication systems. Over the last decade the annual global internet protocol (IP) traffic has been rising at an enormous rate and is going to increase further. Overall IP traffic will grow at a compound annual growth rate of 21% from 2013-2018 [1], resulting in a doubling of the overall traffic in ~3.3 years. The total annual global IP traffic is expected to surpass the zettabyte (1000 exabytes) threshold in 2016 [1].

This ongoing traffic expansion can be attributed to several reasons: More and more devices are connected to the internet, e.g. smart phones, TVs, machines, computers, etc. New concepts such as Industry 4.0 or Smart Home accelerate this trend even more. A key factor for the increased traffic is video content. Furthermore, there is the need for low latency, which in turn requires the content delivery networks and data centers, respectively, moving closer to the user.

In order to cope with this increasing demand for high data rates, the optical networks behind need to be upgraded. The data rates can be increased by using higher-order modulation formats or by increasing the bandwidth. Furthermore, multiplexing techniques as polarization division multiplexing or wavelength/frequency division multiplexing can be utilized to further enhance the data rate.

For today's communications systems, flexible transmitters (Tx) based on digital-to-analog converters (DACs) are desirable. They are able to vary the modulation bandwidth and the modulation format of the transmitted signal. Furthermore, pre-equalization can be used in order to cancel channel impairments and thus, enable transmission at higher data rates.

The circuit technologies impose limitations on the total bandwidth achievable by a single DAC. Therefore, the concept of parallelization (resp. interleaving) has been introduced into the system design. Interleaving for DAC-based Tx can be applied in three ways:

1. Multiplexing DAC (MUXDAC) [2], [3],
2. Time Interleaving DAC (TIDAC) [4], [5] and
3. Frequency Interleaving DAC.

The MUXDAC as well as the TIDAC concept are introduced in Sec. 3. The frequency interleaving approach is based on a concept for oscilloscopes called "digital bandwidth interleaving" and has been introduced by Pupalakis [6], [7]. In this concept, an electrical signal is split in the frequency domain with a special filter into several sub-bands, each having a bandwidth that can be handled by the analog-to-digital converters (ADCs). Thereby, higher frequency bands are down-converted in order to match the bandwidths of the ADCs. In the digital domain, the spectral sub-bands, each being received separately by an

ADC, are digitally recombined to recover the original signal. Thus, a signal with a bandwidth greater than the bandwidths of the individual ADCs can be received. Since the bandwidth interleaving concept has not yet been utilized at the Tx, this paper covers for the first time the required modifications and evaluates the performance for application at the Tx. In accordance with the concept for oscilloscopes, where the spectral sub-bands are split in the analog domain and combined digitally, it is straight-forward to call this scheme "analog bandwidth interleaving" (ABI), since the splitting is performed digitally and the combining or interleaving of the spectral sub-bands is performed in the analog domain. Note, that the concept is rather based on a bandwidth aggregation than on a bandwidth interleaving. The paper is structured as follows. First, the time domain concepts, namely TIDAC and MUXDAC, are presented and evaluated regarding their bandwidth enhancement capabilities. Then, the principle of ABI is introduced for the case of two DACs at the Tx for arbitrary waveforms. Because the two sub-bands overlap, we discuss the use of a multiple-input multiple-output (MIMO) digital signal processing (DSP) algorithm to ensure the proper analog summation of the frequency sub-bands. Moreover, the algorithm includes pre-compensation of the impairment effects introduced by the involved analog components. Experimental results are presented demonstrating the feasibility of bandwidth interleaving at the Tx.

2 D/A Conversion

A DAC is a device that transforms a digital signal $d(n)$ into an analog signal $s(t)$. Ideally, the DAC would produce infinitely sharp pulses. However, this is not realizable by analog components. Therefore, the output value is kept constant for the sample time T_s . This mode of operation is called zero order hold (ZOH) or non-return-to-zero (NRZ). Mathematically formulated the output of the DAC is given by

$$s(t) = \text{rect}\left(\frac{t - T_s/2}{T_s}\right) * \sum_{n=-\infty}^{+\infty} d(n) \cdot \delta(t - nT_s), \quad (1)$$

with

$$\text{rect}\left(\frac{t}{T_s}\right) = \begin{cases} 1, & |t| < T_s/2 \\ \frac{1}{2}, & |t| = T_s/2 \\ 0, & \text{else,} \end{cases} \quad (2)$$

where $\delta(t)$ is the Dirac function and $*$ denotes the convolution operation. In the frequency domain, this operation can be described by a sinc-function with a linear phase on account of a causal system:

$$H_{\text{DAC}}(f) = \mathfrak{F}\{h_{\text{DAC}}(t)\} = T_s \cdot \text{sinc}(\pi f T_s) \cdot e^{-j\pi f T_s}. \quad (3)$$

The frequency response of the ZOH-DAC is visualized in **Fig. 1** by the blue curve. Furthermore, the generated image replica due to the periodic nature of the discrete spectrum are shown. With an appropriate low pass filter (LPF) the signal spectrum in the first Nyquist zone, containing the low-frequency components, has to be selected in order to

remove image bands. Usually, this is not completely possible due to the filter's finite roll-off. Thus, frequency components $f > f_s/2$ remain. Note, that the images in the even Nyquist zones are mirror images (inverted frequency axis orientation) and the images in the odd Nyquist zones are regular images (right frequency axis orientation).

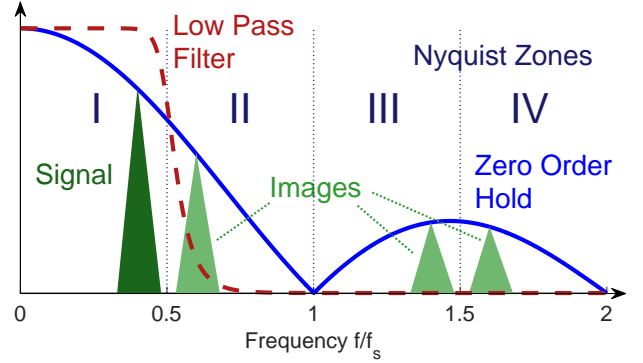


Figure 1 ZOH DAC frequency response (light blue) with Nyquist zones I-IV (dark blue); Generated signal spectrum (dark green) and generated image replicas of the original spectrum (light green); Realizable LPF (dotted red).

3 Time Interleaving Concepts

In the time domain, there are two concepts achieving a performance enhancement for DACs. The first concept is using an analog power combiner in order to sum signals of multiple DACs as shown in **Fig. 2** on the left side and the second one makes use of a multiplexer (MUX) in order to aggregate signals of multiple DACs as shown in **Fig. 2** on the right side. Both concepts are evaluated regarding their ability to increase the sample rate and the bandwidth.

The concept using an analog power combiner in order to sum signals of multiple DACs is shown in **Fig. 2** on the left side. The signals of the individual DACs are exposed to a phase shift relative to each other in order to guarantee a correct summation. Furthermore, one can distinguish between two techniques as shown in **Fig. 2 (b)**: firstly, NRZ signals can be added. However, they require a digital pre-compensation algorithm to calculate the individual sequences contributing to the combined signal. This variant is also known as pseudo-interleaving and used e.g. in the Fraunhofer HHI Arbitrary Waveform Generator (AWG) with 70 GS/s and 18 GHz bandwidth [8]. Secondly, return-to-zero (RZ) signals can be used, which do not require a pre-compensation algorithm, as shown in **Fig. 2 (b)**. Hence, this technique is called true interleaving [4]. However, the requirements on the DAC's switching speed are increased. Both techniques increase the sample rate N -fold by using N DACs, but the bandwidth remains constant, since the combined DAC is limited by each DAC's sinc-roll-off in the frequency domain.

The other concept in the time domain makes use of a high-speed MUX as shown in **Fig. 2** on the right side. Multiple DACs generate analog signals, which are then aggregated to a higher sample rate with a high-speed analog MUX, which switches between the input signals. In **Fig. 2 (d)** the ideal MUX operation is shown for the case of two DACs. The MUX output is generated by switching between the two input signals, whereby the MUX "samples" the input signals in the center of each symbol, which is denoted by the black dotted line.

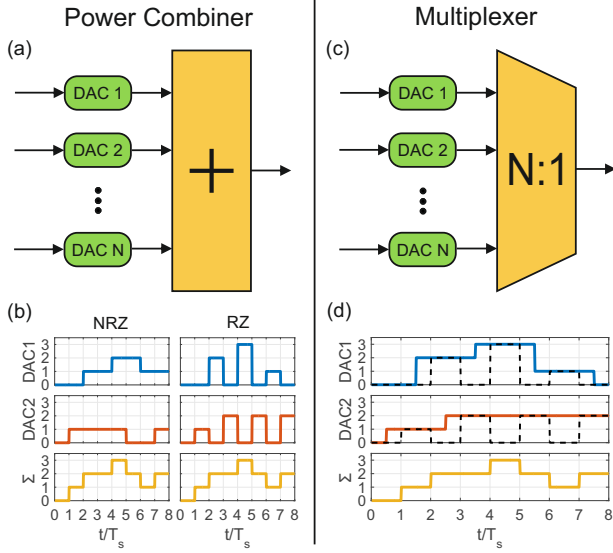


Figure 2 DAC time interleaving concepts: TIDAC (a); NRZ and RZ signaling for TIDAC (b); MUXDAC (c); MUXDAC operating principle (d).

The MUX does not necessarily be a single MUX - a multi stage approach consisting of several MUXs is possible as well. Recently, an 80 GBd DAC has been shown [3] by aggregating the output of two DACs with an analog multiplexer. The sample rate is increased N -fold by using N DACs. The bandwidth, however, is determined mainly by the bandwidth of the analog MUX and thus, the bandwidth limitations of the DACs can be circumvented.

The time interleaving concepts introduced need technological advances in order to achieve a performance improvement. The TIDAC concept requires advances in the underlying DAC design to achieve a performance improvement, whereas the MUXDAC approach requires improvements in the design of external high-speed MUXs. In this paper, we propose a concept, that can be realized with existing analog components in order to enhance the performance of DACs: analog bandwidth interleaving. A digital pre-equalization algorithm enables the bandwidth enhancement without requiring technological advances.

4 Analog Bandwidth Interleaving (ABI) System Overview

The idea behind analog bandwidth interleaving (ABI) is to perform the digital-to-analog (D/A) conversion of the

input signal $d(n)$ with multiple D/A converters in parallel instead of using a single converter; a first block diagram has been shown in [9]. Thereby, each DAC performs the D/A conversion for a spectral fraction of the input signal $d(n)$. These spectral fractions are then converted back to their native frequency locations by means of analog processing, e.g. mixers and filters, in order to generate the analog representation $s(t)$ of the digital signal $d(n)$, which has a total bandwidth greater than the bandwidth of the incorporated DACs. In principle, the concept is realizable with an arbitrary amount of DACs, but for an easier comprehension and analysis the figures and explanations are restricted to two DACs. Note, that with this approach an arbitrary waveform can be generated in the analog domain contrary to [10], where a similar approach is conducted, though, being limited to discrete multi tone and orthogonal frequency division multiplexing waveforms.

In **Fig. 3** an overview of the system is shown as a block diagram for the case of two DACs. The system consists of a digital part (light blue area) and an analog part (light red area). The digital signal processing is performed as follows: the $2N$ -point data sequence $\mathbf{d} = [d(0), d(1), \dots, d(2N-1)] \in \mathbb{R}$ undergoes a discrete Fourier transform (DFT) and the corresponding two-sided spectrum is given by $\mathbf{D} = \mathcal{F}_{\text{DFT}}\{\mathbf{d}\} = [\mathbf{D}^+, \mathbf{D}^-]$ as shown in **Fig. 3 (a)**. The plus and minus superscript denote the positive and the negative frequency range of the spectrum, respectively. In **Fig. 3 (a)** the direction of frequency is additionally given by the arrows in the spectra. The spectrum \mathbf{D} is split into two parts \mathbf{D}_1 and \mathbf{D}_2 , denoted in **Fig. 3 (b)** as **I** and **II**, while considering positive and negative frequencies:

$$\mathbf{D} = [\mathbf{D}^+, \mathbf{D}^-] = [\mathbf{D}_1^+, \mathbf{D}_2^+, \mathbf{D}_2^-, \mathbf{D}_1^-] \quad (4)$$

$$\mathbf{D}_1 = [\mathbf{D}_1^+, \mathbf{D}_1^-] \quad (5)$$

$$\mathbf{D}_2 = [\mathbf{D}_2^+, \mathbf{D}_2^-]. \quad (6)$$

The splitting operation corresponds to a brick-wall or ideal filtering of the lower sideband and both a brick-wall or ideal filtering and implicit downconversion of the upper sideband - a digital local oscillator (LO) is not mandatory. Other splitting approaches such as raised cosine filtering are possible as well, but they introduce overhead and thus reduce the overall achievable bandwidth. Though, they might improve the time domain behavior, since the impulse response is limited in length.

Having obtained the two data spectra, MIMO pre-equalization is performed. The equalization procedure is explained in detail in Sec. 6. The corresponding time domain signals $x_1(n)$ and $x_2(n)$ of the pre-equalized spectra $X_1(k)$ and $X_2(k)$ are obtained with an inverse discrete Fourier transform (IDFT) and are fed to the DACs as shown in **Fig. 3 (d)**. Note, that the second spectrum will be inverted in frequency prior to the IDFT, if the lower sideband of the mixer output is used as shown in **Fig. 3 (c)** and **(h)**.

The DACs are running at their maximum sample rate f_s without oversampling in order to generate the analog

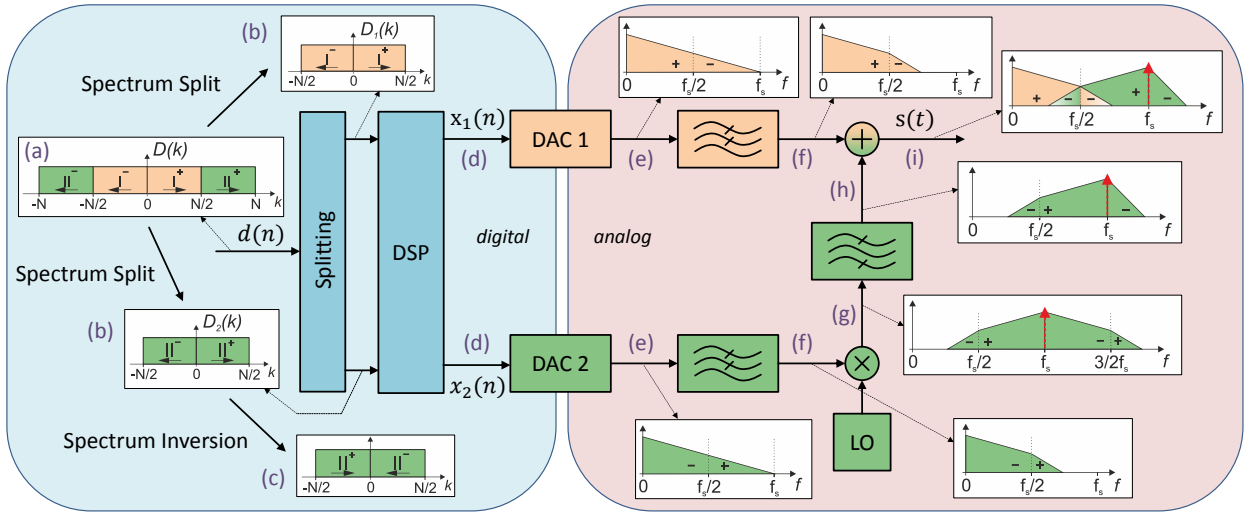


Figure 3 The concept of ABI as a block diagram for two DACs: a digital sequence is split in the frequency domain into two parts and processed by digital signal processing algorithms. The second spectrum (green) is further inverted in frequency in account of using the lower mixer side band. After D/A conversion both signals are low pass filtered. The second signal is upconverted to its native location and one of the sidebands is filtered with an appropriate band pass filter. Both signals are finally recombined.

signals. Due to the rectangular pulse shape of the DACs, the spectra of the DACs' outputs are attenuated by the sinc-function, which is illustrated as triangles in **Fig. 3 (e)**. The frequency images need to be removed by appropriate LPFs. These filters are not able to remove all image components due to their finite roll-off as shown in **Fig. 3 (f)**. Now, analog processing of the signal in the first path is finished and the second signal undergoes more analog processing steps.

The second signal is multiplied by the LO, in order to shift it to a higher frequency region (**Fig. 3 (g)**). Two alternatives exist for the position of the LO: either the LO is located at half of the DACs' sampling frequency $f_s/2$ or directly at the sampling frequency f_s . For the second alternative, as shown in the figure, the spectrum has to be digitally inverted prior to D/A conversion (**Fig. 3 (c)**) in order to obtain the right frequency orientation in the upper band at the end. The upconversion with a cosine carrier generates two side bands. One of these side bands is unnecessary and has to be removed by a band pass filter (**Fig. 3 (h)**).

Finally, the two individual signals are combined, e.g. with a passive power combiner, in order to form an analog representation $s(t)$ of the digital signal $d(n)$ with a bandwidth of f_s and a sampling rate of $2f_s$ (**Fig. 3 (i)**).

5 System Model

In order to pre-compensate the channel distortions, a model for the discrete channel consisting of the analog parts shown in the light red area in **Fig. 3** is developed. This opens the possibility to apply DSP undoing the channel distortions and hence, to achieve a good-quality output signal. The combined signal shown in **Fig. 3 (i)** is affected by crosstalk between the frequency bands around $f_s/2$ and

frequency components located at frequencies $f > f_s$. The spectral components of the sum signal can be altered in the frequency regions $[0, f_s/2]$ by the first DAC and $[f_s/2, f_s]$ by the second DAC due to the frequency upconversion. Frequency components located at frequencies $f > f_s$ cannot be directly modified. However, the undesired components at $f > f_s$ can be shaped by an appropriate filter or removed by means of oversampling in combination with an appropriate filter having a steep roll-off. Thus, we focus on the crosstalk between the frequency bands. In or-

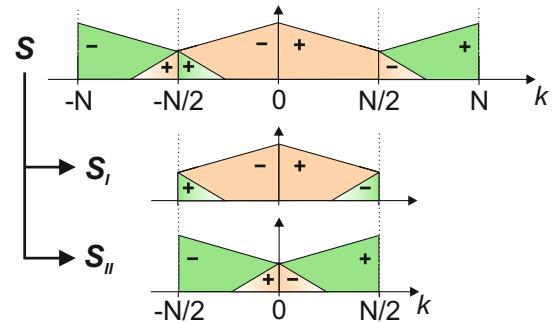


Figure 4 Separating the spectrum S into two individual components S_I and S_{II} .

der to obtain a channel model the sum signal at the output $s(t)$ is ideally sampled with a sampling rate of $2f_s$ yielding the digital signal $s(n)$ restricted to the frequency range of $[-f_s, +f_s]$. The spectral representation $S = \mathcal{F}_{\text{DFT}}\{s(n)\}$ is illustrated in **Fig. 4**. Despite $s(n)$ being a real-valued signal, the two-sided spectrum is shown here instead of the single-sided spectrum, since the DFT yields a two-sided spectrum. The spectrum S is split into a lower frequency band S_I and an upper frequency band S_{II} , as has been done before in (4) to (6):

$$\mathbf{S} = [\mathbf{S}^+, \mathbf{S}^-] = [\mathbf{S}_I^+, \mathbf{S}_{II}^+, \mathbf{S}_I^-, \mathbf{S}_{II}^-] \quad (7)$$

$$\mathbf{S}_I = [\mathbf{S}_I^+, \mathbf{S}_I^-] \quad (8)$$

$$\mathbf{S}_{II} = [\mathbf{S}_{II}^+, \mathbf{S}_{II}^-]. \quad (9)$$

Now, there are two signal spectra that can be individually modified by the DACs: \mathbf{S}_I by the first DAC and \mathbf{S}_{II} by the second DAC. In the following, the individual frequency components of the spectra become important. Thus, the notation refers to $S(k)$ instead of \mathbf{S} , where k denotes the discrete frequency.

The combined output signal $s(t)$ (**Fig. 3 (i)**) should be a correct representation of the digital input signal $d(n)$ (**Fig. 3 (a)**). However, there are crosstalk terms distorting the signal, which need to be undone in order to reconstruct the digital signal properly.

Another representation of the spectra $S_I(k)$ and $S_{II}(k)$ is shown in **Fig. 5**. The spectra $S_I(k)$ and $S_{II}(k)$ are each separated into the desired main components $H_{11}(k)X_1(k)$ and $H_{22}(k)X_2(k)$ and the undesired crosstalk components $H_{12}(k)X_2(k+N/2)$ and $H_{21}(k)X_1(k+N/2)$. Note, that X_i are the spectral representations of the signals being fed to the DACs and H_{ij} are the channel frequency responses characterizing the MIMO channel from the DACs to the combined output with $i, j \in 1, 2$. If the system is treated as

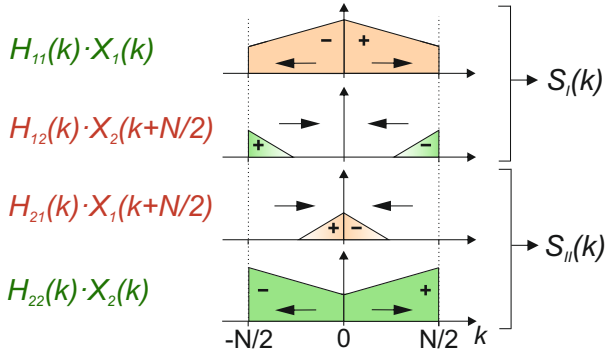


Figure 5 Received spectra $S_I(k)$ and $S_{II}(k)$ with their desired components (dark green) and their undesired components (dark red).

a MIMO system, the cross-coupling between the channels can be modeled as a linear system in the frequency domain. Unfortunately, the description as a standard MIMO problem fails. Considering the arrows in **Fig. 5**, denoting the direction of frequency, it can be observed, that the crosstalk components are reversed in frequency. Thus, a regular MIMO model is not appropriate, because it does not cover frequency inversion. Hence, the MIMO model has to be modified in order to include these additional operations in the frequency domain.

The actual problem encompasses cross-coupling terms, $H_{12}(k)X_2(k+N/2)$ and $H_{21}(k)X_1(k+N/2)$, which are the mirror spectra of the actual spectra. The arrows in **Fig. 5**, which denote the direction of frequency, visualize that the spectra are reversed in frequency and complex conjugated.

This operation can be described by a shift of half of the sample points of the DFT: $X(k+N/2) = X(k-N/2)$, exploiting the repetitive nature of the discrete spectrum. This operation has been shown in another context in **Fig. 3 (b)** to **(c)**.

The cross-coupling problem, which arises due to the non-ideal filtering as shown in **Fig. 5**, is denoted as

$$S_I(k) = H_{11}(k) \cdot X_1(k) + H_{12}(k) \cdot X_2(k+N/2) \quad (10)$$

$$S_{II}(k) = H_{21}(k) \cdot X_1(k+N/2) + H_{22}(k) \cdot X_2(k), \quad (11)$$

where $X_1(k)$ and $X_2(k)$ are the spectra after the equalizer. This MIMO system is visualized in **Fig. 6**. The difference to the standard 2×2 MIMO problem becomes obvious by two additional shift operations in the frequency domain.

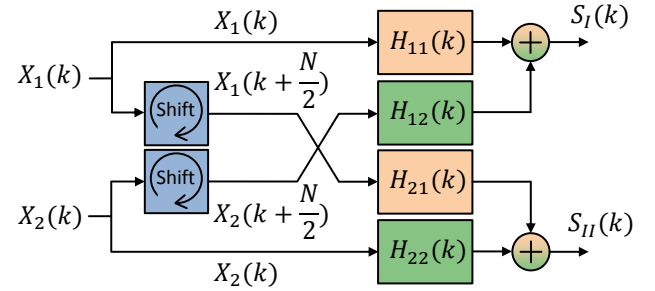


Figure 6 MIMO channel model block diagram with two additional shift operations.

The 2×2 MIMO model is a linear system of equations given by (8) and (9). Following [11], where a similar mathematical problem was faced in another context, the crosstalk can be modeled as a 4×4 MIMO channel as shown in Appendix A. Thereby, a compact solution can be achieved by matrix inversion.

Note, that by using oversampling, the crosstalk between the two frequency bands could be almost completely avoided due to analog filters rather than digital signal processing. However, the achievable bandwidth enhancement is reduced.

6 Digital Signal Processing

With the developed MIMO channel model shown in **Fig. 6**, an equalizer with coefficients $W_{ij}(k)$, operating in the digital domain in **Fig. 3** (light blue area), can be designed. This equalizer undoes the crosstalk and the frequency response mismatches introduced by the analog components in **Fig. 3** (light red area).

The DSP steps for frequency domain equalization (FDE) utilizing a repetitive data sequence, e.g. in an AWG, are shown in **Fig. 7**. The sequence $d(n)$ is transformed to the frequency domain with a fast Fourier transform (FFT). Then, it is split into two parts $D_1(k)$ and $D_2(k)$. A shifted and a non-shifted version of $D_1(k)$ and $D_2(k)$ are generated. The equalizers $W_{ij}(k)$ are applied to the spectra $D_j(k)$ and $D_j(k+N/2)$ with $i, j \in \{1, 2\}$. The resulting spectra are transformed back to the time domain via an inverse fast

Fourier transform (IFFT) operation and the resulting sequences can be fed to the DACs. The equalizer coefficients

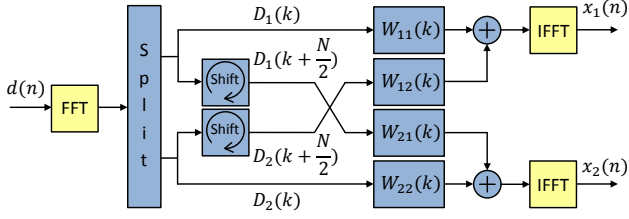


Figure 7 MIMO DSP steps: The input signal undergoes an FFT, is split in the Fourier domain and equalized by a MIMO equalizer with two additional shift operations. Each output of the MIMO equalizer undergoes an IFFT.

$W_{ij}(k)$ with $i, j \in \{2, 2\}$ are given by the solution for the 4×4 MIMO problem in Appendix A.2.

If a continuous data stream, rather than a repetitive data sequence is used, additional techniques are necessary for FDE such as overlap-add or overlap-save [12]. Note, that a time domain equalizer would enable continuous operation without additional techniques.

7 Experimental Results

In order to verify the proposed DSP algorithm, initial experiments were conducted with low-speed DACs under laboratory conditions. The setup as shown in **Fig. 8** is

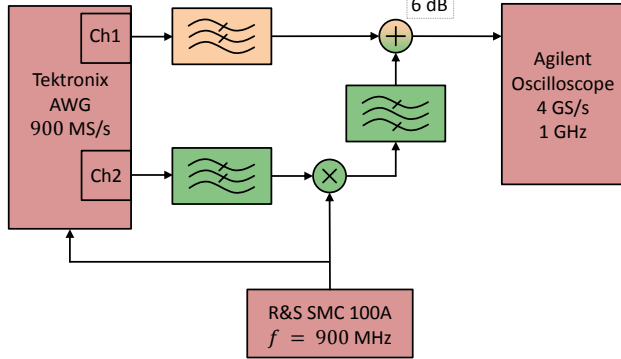


Figure 8 Experimental setup: an AWG generates two signals, which undergo analog processing by means of filters and a mixer. The signals are finally combined and captured by an oscilloscope.

utilized. For the D/A conversion, an arbitrary waveform generator *Tektronix AWG5012* with 14 bits nominal vertical resolution is used at a sample rate of 900 MS/s provided by an external clock. The LPFs following the DACs are *MiniCircuits SLP-450* with cutoff frequency $f_c = 440$ MHz. The mixer *MiniCircuit ZFM-150-S* is driven by a 900 MHz local oscillator (LO) with 10 dBm power provided by the signal generator *Rohde und Schwarz SMC 100A*. The LO signal drives the AWG as well in order to achieve phase stability between these devices. In lack of an appropriate band pass filter a combination of an LPF *SLP-850* with $f_c = 850$ MHz and high pass filter *SHP-500*

with $f_c = 454$ MHz was used to filter the undesired mixer sideband. The signals of the first and the second signal path are combined by means of the passive power combiner *MiniCircuit ZX10R-14* and acquired with the real-time oscilloscope *Agilent MSO 7104A* with 4 GS/s, 1 GHz analog bandwidth and 8 bit vertical resolution. The oscilloscope and the signal generator are synchronized with a 10 MHz reference clock. The signal amplitudes are roughly matched by inserting attenuators in the first path. Due to reflections at the power combiner, additional attenuators are inserted in the setup order to reduce these reflections.

At first, a channel estimation is conducted in order to estimate the crosstalk and the frequency responses of the analog components in a joint manner. A De Bruijn binary sequence (DBBS) of length 16384 is generated in MATLAB. The sequence is Fourier transformed and split into two fractions. The second spectrum is shifted by 8192 samples. Then, both spectra are passed through an inverse Fourier transform and fed to the DACs. Thus, two spectral fractions are generated each occupying a range of 450 MHz: the first one in the baseband from 0 to 450 MHz and the second one in the passband from 450 MHz to 900 MHz. After capturing the combined signal with the scope, a least squares MIMO channel estimation with 512 taps yields the result shown in **Fig. 9**. There are two channel frequency responses visible, whereby the orange line represents the channel from the first DAC to the combined output and the green line represents the channel from the second DAC to the combined output. We observe a strong roll-off, which can be attributed to the AWG's limited bandwidth of 250 MHz. The crossing point of the frequency responses is roughly at 450 MHz as intended. The frequency responses need to be raised by 20 dB in order to undo the channel characteristics, which is achieved by the developed DSP MIMO algorithm as well. The channel impairments need

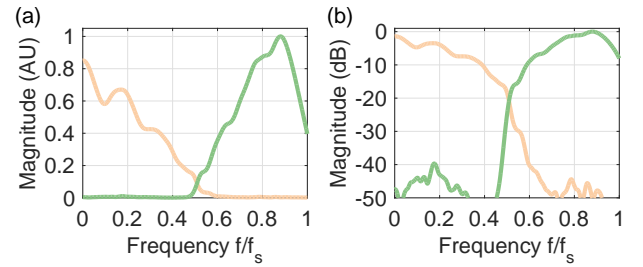


Figure 9 ABI channel frequency responses for the experimental setup in linear scale (a) and logarithmic scale (b): DAC 1 \rightarrow LPF \rightarrow combined output (orange) and DAC 2 \rightarrow LPF \rightarrow mixer \rightarrow BPF \rightarrow combined output (green).

to be undone in order to generate the desired output signal. Therefore, a DBBS sequence of length 131072 is generated in MATLAB. The sequence is Fourier transformed and split into two fractions. These two spectral fractions are pre-equalized according to the ZF-algorithm presented in Sec. 6 in order to cancel crosstalk between the frequency bands. The MIMO channel frequency response obtained in the previous step was interpolated to match the sequence

length in order to apply FDE. However, in order to filter the upper sideband at frequencies $> f_s$, without distorting the actual signal spectrum, oversampling needs to be applied to the signal: the signal is pre-processed such that the combined signal has an oversampling ratio of 1.125, achieving a total bandwidth of 800 MHz and a symbol rate of 1600 MBd. The second spectral fraction is shifted by half of the number of sample points in order to use the lower sideband of the mixer output. After the IFFT, the corresponding time domain sequences are fed to the DACs. The magnitudes of both spectral fractions are roughly matched by attenuators inserted in the setup. However, for a fine tuning the AWG's output amplifier levels are adjusted manually, such that both spectra have an equal magnitude.

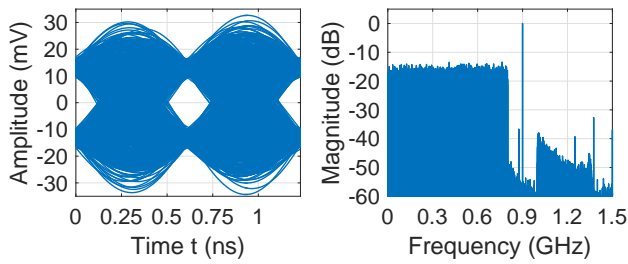


Figure 10 Eye diagram and spectrum for ABI with two DACs running at 900 MS/s generating a signal with 1600 MBd and 800 MHz total bandwidth.

The spectrum of the resulting signal as well as the corresponding eye diagram are visualized in **Fig. 10**. A clear eye opening is visible, though the eye amplitude is small, i.e. < 40 mV. This power loss is attributed mainly to the attenuators in the setup, the passive power combiner and the limited bandwidth of the AWG. A flat spectrum, corresponding to a sinc pulse shape in the time domain, can be observed from 0 to 800 MHz. Due to oversampling the upper sideband is moved to a higher frequency beginning at 1 GHz. The mixer LO at 900 MHz has a magnitude almost 15 dB greater than the magnitude of the signal.

8 Conclusion and Outlook

In this paper interleaving concepts for DACs were reviewed and a new frequency interleaving approach was presented for the first time ever. A MIMO DSP algorithm was presented canceling the inherent crosstalk between the frequency bands. Major requirement for the functionality of the system are phase stability between the LO and the DAC clock, components with flat frequency responses and high resolution DACs. The successful interleaving of two frequency bands was shown for low-speed DACs experimentally.

As a next step, the concept needs to be investigated with high-speed DACs. It is expected that the vertical resolution, i.e. 6-8 bits, will limit the performance of the proposed method, since simulation results showed that a high resolution is necessary. Moreover, a greater bandwidth of multiple 10s of GHz will introduce more noise into the system restraining the overall system performance. Another

research direction is aiming at nonlinear pre-distortion algorithms in order to improve the performance of the system.

9 References

- [1] Cisco Systems Inc., “Cisco visual networking index,” Cisco Systems Inc., Tech. Rep., June 2014.
- [2] M. Nagatani, H. Wakita, H. Nosaka, K. Kurishima, M. Ida, A. Sano, and Y. Miyamoto, “75 gbd inp-hbt mux-dac module for high-symbol-rate optical transmission,” *Electronics Letters*, vol. 51, no. 9, pp. 710–712, 2015.
- [3] H. Yamazaki, M. Nagatani, S. Kanazawa, H. Nosaka, T. Hashimoto, A. Sano, and Y. Miyamoto, “160-gbps nyquist pam4 transmitter using a digital-preprocessed analog-multiplexed dac,” in *Optical Communication (ECOC), 2015 European Conference on*. IEEE, 2015, pp. 1–3.
- [4] H. Huang, J. Heilmeyer, M. Grozing, M. Berroth, J. Leibrich, and W. Rosenkranz, “An 8-bit 100-gs/s distributed dac in 28-nm cmos for optical communications,” *Microwave Theory and Techniques, IEEE Transactions on*, vol. 63, no. 4, pp. 1211–1218, 2015.
- [5] Fujitsu, “Leia 55 - 65 gsa/s 8-bit dac factsheet,” 2012. [Online]. Available: <http://www.fujitsu.com/downloads/MICRO/fme/documentation/c60.pdf>
- [6] P. Pupalais, “Digital bandwidth interleaving,” LeCroy Corporation, White Paper, 2005.
- [7] LeCroy Corporation, “The interleaving process in digital bandwidth interleaving (dbi) scopes,” LeCroy Corporation, White Paper, 2009.
- [8] Fraunhofer HHI, “Fraunhofer hhi awg flyer,” 2013. [Online]. Available: <http://hhi.fraunhofer.de/70awg>
- [9] C. Laperle and M. O’Sullivan, “Advances in high-speed dacs, adcs, and dsp for optical coherent transceivers,” *Lightwave Technology, Journal of*, vol. 32, no. 4, pp. 629–643, Feb 2014.
- [10] C. Kottke, K. Habel, C. Schmidt, and V. Jungnickel, “154.9 gb/s ofdm transmission using im-dd, electrical iq-mixing and signal combining,” in *National Fiber Optic Engineers Conference*. Optical Society of America, March 2016.
- [11] R. M. Rao and B. Daneshrad, “Analog impairments in mimo-ofdm systems,” *Wireless Communications, IEEE Transactions on*, vol. 5, no. 12, pp. 3382–3387, 2006.
- [12] F. Pancaldi, G. Vitetta, R. Kalbasi, N. Al-Dhahir, M. Uysal, and H. Mheidat, “Single-carrier frequency domain equalization,” *Signal Processing Magazine, IEEE*, vol. 25, no. 5, pp. 37–56, September 2008.

A Appendix

In general the MIMO system is described in the frequency domain as

$$\mathbf{S}(k) = \underline{\mathbf{C}}(k)\mathbf{X}(k) + \mathbf{V}(k), \quad (12)$$

where there is an individual equation for each frequency line k . $\mathbf{S}(k)$ is the system output signal, $\mathbf{X}(k)$ is the DAC output signal and $\mathbf{V}(k)$ is the vector of noise samples. These are given by

$$\mathbf{S}(k) = \begin{bmatrix} S_1(k) \\ S_1(k+N/2) \\ \vdots \\ S_L(k) \\ S_L(k+N/2) \end{bmatrix}, \quad \mathbf{X}(k) = \begin{bmatrix} X_1(k) \\ X_1(k+N/2) \\ \vdots \\ X_M(k) \\ X_M(k+N/2) \end{bmatrix}, \quad (13)$$

$$\mathbf{V}(k) = \begin{bmatrix} V_1(k) \\ V_1(k+N/2) \\ \vdots \\ V_L(k) \\ V_L(k+N/2) \end{bmatrix}, \quad (14)$$

where L and M denote the number of receivers and transmitters, respectively. The channel matrix $\underline{\mathbf{C}}(k)$ is therefore defined as

$$\underline{\mathbf{C}}(k) = \begin{bmatrix} C_{1,1}(k) & C_{1,2}(k) & \cdots & C_{1,2M}(k) \\ C_{2,1}(k) & C_{2,2}(k) & \cdots & C_{2,2M}(k) \\ \vdots & \vdots & \ddots & \vdots \\ C_{2L,1}(k) & C_{2L,2}(k) & \cdots & C_{2L,2M}(k) \end{bmatrix}. \quad (15)$$

The pre-equalizer undoing the channel impairments is given by the weight-matrix $\underline{\mathbf{W}}(k)$:

$$\mathbf{X}(k) = \underline{\mathbf{W}}(k)\mathbf{D}(k), \quad (16)$$

where $\underline{\mathbf{W}}(k)$ and the data vector $\mathbf{D}(k)$ are given by

$$\underline{\mathbf{W}}(k) = \begin{bmatrix} W_{1,1}(k) & W_{1,2}(k) & \cdots & W_{1,2L}(k) \\ W_{2,1}(k) & W_{2,2}(k) & \cdots & W_{2,2L}(k) \\ \vdots & \vdots & \ddots & \vdots \\ W_{2M,1}(k) & W_{2M,2}(k) & \cdots & W_{2M,2L}(k) \end{bmatrix}, \quad (17)$$

$$\mathbf{D}(k) = \begin{bmatrix} D_1(k) \\ D_1(k+N/2) \\ \vdots \\ D_L(k) \\ D_L(k+N/2) \end{bmatrix}. \quad (18)$$

A.1 Zero Forcing Equalizer

For a zero forcing (ZF) equalizer the noise is disregarded and thus the received signal is given by

$$\mathbf{S}(k) = \underline{\mathbf{C}}(k)\mathbf{X}(k) \Big|_{\mathbf{V}(k)=0} = \underline{\mathbf{C}}(k)\underline{\mathbf{W}}_{ZF}(k)\mathbf{D}(k) \quad (19)$$

Claiming that $\mathbf{S}(k) \stackrel{!}{=} \mathbf{D}(k)$ to recover the signal there are two solutions depending on the matrix $\underline{\mathbf{C}}(k)$:

1. $\underline{\mathbf{C}}(k)$ is quadratic and invertible:

$$\Rightarrow \underline{\mathbf{W}}_{ZF}(k) = \underline{\mathbf{C}}^{-1}(k) \quad (20)$$

2. $\underline{\mathbf{C}}(k)$ is non-quadratic: Use the well-known Moore-Penrose pseudo inverse for matrix inversion:

$$\Rightarrow \underline{\mathbf{W}}_{ZF}(k) = (\underline{\mathbf{C}}^H(k)\underline{\mathbf{C}}(k))^{-1}\underline{\mathbf{C}}^H(k), \quad (21)$$

where $(\cdot)^H$ denotes the conjugate transpose and $(\cdot)^{-1}$ the inverse.

A.2 4×4 MIMO for ABI

As mentioned in Sec. 5 the system can be modeled as a MIMO problem, where $L = M$ is not necessarily satisfied. However, $L = M$ simplifies the solution and enables an appropriate linear formulation.

In the preferred 4×4 MIMO formulation only half of the entries in the channel matrix $\underline{\mathbf{C}}(k)$ are $\neq 0$, since the other crosstalk terms are not present:

$$\underline{\mathbf{C}}(k) = \begin{bmatrix} H_{11}(k) & 0 & 0 & H_{12}(k) \\ 0 & H_{11}(k+\frac{N}{2}) & H_{12}(k+\frac{N}{2}) & 0 \\ 0 & H_{21}(k) & H_{22}(k) & 0 \\ H_{21}(k+\frac{N}{2}) & 0 & 0 & H_{22}(k+\frac{N}{2}) \end{bmatrix} \quad (22)$$

Thereby, the pre-equalizer is given as

$$\underline{\mathbf{W}}_{ZF}(k) = \underline{\mathbf{C}}^{-1}(k) \quad (23)$$

$$= \text{diag} \left(\begin{bmatrix} \frac{1}{H_{11}(k)H_{22}(k+\frac{N}{2})-H_{12}(k)H_{21}(k+\frac{N}{2})} \\ \frac{1}{H_{11}(k+\frac{N}{2})H_{22}(k)-H_{12}(k+\frac{N}{2})H_{21}(k)} \\ \frac{1}{H_{11}(k+\frac{N}{2})H_{22}(k)-H_{12}(k+\frac{N}{2})H_{21}(k)} \\ \frac{1}{H_{11}(k)H_{22}(k+\frac{N}{2})-H_{12}(k)H_{21}(k+\frac{N}{2})} \end{bmatrix} \right) \cdot \begin{bmatrix} H_{22}(k+\frac{N}{2}) & 0 & 0 & -H_{12}(k) \\ 0 & H_{22}(k) & -H_{12}(k+\frac{N}{2}) & 0 \\ 0 & -H_{21}(k) & H_{11}(k+\frac{N}{2}) & 0 \\ -H_{21}(k+\frac{N}{2}) & 0 & 0 & H_{11}(k) \end{bmatrix} \quad (24)$$

Note, that only the first row and the third row are relevant, since the second and the fourth row contain the same frequency domain signals shifted by $N/2$. The result is given as:

$$W_{11}(k) = \frac{H_{22}(k+\frac{N}{2})}{H_{11}(k)H_{22}(k+\frac{N}{2})-H_{12}(k)H_{21}(k+\frac{N}{2})} \quad (25)$$

$$W_{14}(k) = -\frac{H_{12}(k)}{H_{11}(k)H_{22}(k+\frac{N}{2})-H_{12}(k)H_{21}(k+\frac{N}{2})} \quad (26)$$

$$W_{32}(k) = -\frac{H_{21}(k)}{H_{11}(k+\frac{N}{2})H_{22}(k)-H_{12}(k+\frac{N}{2})H_{21}(k)} \quad (27)$$

$$W_{33}(k) = \frac{H_{11}(k+\frac{N}{2})}{H_{11}(k+\frac{N}{2})H_{22}(k)-H_{12}(k+\frac{N}{2})H_{21}(k)} \quad (28)$$

Mapping this formulation to the equalizer shown in **Fig. 7**, we get $W_{11,\text{fig}}(k) = W_{11}(k)$, $W_{12,\text{fig}} = W_{14}(k)$, $W_{21,\text{fig}} = W_{32}(k)$ and $W_{22,\text{fig}} = W_{33}(k)$.